IEEE Access
Multidisciplinary : Rapid Review : Open Access Journal

Received December 15, 2021, accepted January 14, 2022, date of publication January 27, 2022, date of current version May 13, 2022.

Digital Object Identifier 10.1109/ACCESS.2022.3146941

Space Efficient Meta-Grid Lines for Mutual Coupling Reduction in Two-Port Planar Monopole and DRA Array

MOHIT MISHRA[1], (Graduate Student Member, IEEE), SUMANTRA CHAUDHURI[2], RAKHESH SINGH KSHETRIMAYUM[1], (Senior Member, IEEE), AROKIASWAMI ALPHONES[3], (Senior Member, IEEE), AND KARU P. ESSELLE[4], (Fellow, IEEE)

[1]Department of Electronics and Electrical Engineering, IIT Guwahati, Guwahati 781039, India
[2]School of Engineering, Presidency University, Bengaluru, Karnataka 560064, India
[3]School of Electrical and Electronic Engineering, Nanyang Technological University, Singapore 639798
[4]School of Electrical and Data Engineering, University of Technology Sydney, Ultimo, NSW 2007, Australia

Corresponding author: Mohit Mishra (mohit.mishra@iitg.ac.in)

This work was supported by the Indian Institute of Technology Guwahati, Guwahati, India.

ABSTRACT Traditionally used mutual coupling (MC) reduction techniques such as electromagnetic bandgap structures, isolators and neutralization lines require extra space between radiators. Besides, metamaterial-based techniques require multi-layer arrangements. However, the proposed meta-grid lines overcomes the above demerits by integrating meta-grid lines in the ground plane itself. As a proof-of-concept, two-port CPW-fed monopole antenna array (TPCFMAA) and two-port DRA array (TPDRAA) are designed, fabricated and tested. It has been observed that the TPCFMAA has mutual coupling below -20 dB for frequency between 2.6 to 4.4 GHz. The envelope correlation coefficient reduces from 0.072 to 0.026 by integrating meta-grid lines in the ground plane of the TPCFMAA. At 3.5 GHz, the inter-element distance between the antennas is noted to be $\mathbf{0.015}\lambda_\mathbf{h}$ ($\lambda_\mathbf{h}$ = highest operating wavelength). The TPDRAA's operating frequency can be tuned by changing the parameters of the annular ring slot in the excitation patch. The bandwidth of TPDRAA can be further increased by merging the two resonances of the two annular ring slots in the excitation patch. For TPDRAA, the measured -10 dB impedance bandwidth is from 5.65 to 6.55 GHz. The mutual coupling between the antenna elements is seen to be below -16 dB for an inter-element spacing of 4.8 mm, which is $0.090\lambda_\mathbf{h}$. The measured gain of TPDRAA within the bandwidth is from 4.17 dBi to 5.2 dBi. The TPCFMAA can be used in 3.5 GHz Internet of Vehicles (IoV) multi-user MIMO service, whereas the TPDRAA can be used for satellite communication in the 5.925 to 6.425 GHz frequency band, WiMAX in the 5.7 to 5.85 GHz band, ISM in the 5.725 to 5.85 GHz band, and WLAN in the 5.8 GHz band.

INDEX TERMS MIMO antenna, CPW-fed printed monopole antenna array, cylindrical dielectric resonator antenna (CDRA) array, single negative (SNG) meta-grid lines.

I. INTRODUCTION

Multiple-input-multiple-output (MIMO) communication system fulfills the demand for higher data rate and better quality of service in modern communication systems. MIMO system's channel capacity increases linearly with the number of the antenna elements for rich Rayleigh scattering environments [1], [2]. Compact MIMO communication systems generally deploy closely spaced multiple antennas at the transmitter and receiver sides. However, this results in an undesired mutual coupling (MC) effect, which is inversely proportional to the distance between the antenna array elements [3]. Therefore, designing a compact MIMO antenna with small inter-element spacing and low mutual coupling between antenna array elements is challenging.

In the literature, several methods have been proposed to reduce the MC between planar and dielectric resonator antenna (DRA) elements. For MC reduction in planar antennas, electromagnetic band gap (EBG) [4] structures in [5]–[9]

The associate editor coordinating the review of this manuscript and approving it for publication was Giorgio Montisci.

and isolators in [10] and [11] are used. Neutralization Lines (NLs) are used for isolation enhancement in [12] and [13] for planar monopole antennas. However, EBG structures, isolators and NLs require extra space between the antenna elements and therefore increase the inter-element spacing between them. Mushroom type EBG unit cells used for MC reduction in [5], are spread on 13.5 mm × 48.5 mm space. EBG surface composed of short-circuited microstrips is used in [6] for MC reduction and occupies two times more area than that of the single radiating patch. Uniplanar compact EBG structure of 13.2 mm × 72.6 mm size is used in [7] for MC reduction in another layer that also increases the vertical profile of the two-port antenna by 1.27 mm. In [8], EBG unit cells occupy 33.3 % of the total antenna area. EBG based fractal isolator is used for MC reduction in [9], which takes a size of 16 mm × 23 mm while the single radiating patch occupies a space of 23 mm × 23 mm. Similarly, NLs and isolators also occupy area which increase the edge-to-edge spacing between antenna elements. A ring-shaped defected ground structure is demonstrated to suppress the MC between two cylindrical DRAs (CDRAs) in [14]. In [15], mushroom-shaped DRAs are arranged orthogonally to reduce the MC between them. Triple-port, two-element CDRA with orthogonal modes for MIMO applications is presented in [16]. Two-port low MC antenna array comprising two A-shaped DRAs are excited by means of conformal strip for wideband applications in [17]. Three decoupled modes in a single rectangular DRA are excited using three separate ports to achieve low inter-port coupling in [18]. Metal strips are printed on the dielectric block (DB) in [19] and vias are inserted in the DBs in [20] for enhancing the decoupling. Exotic properties of metamaterials have been exploited for MC reduction [21]–[25]. Waveguide metamaterial (MTM) is placed in the same layer as that of patches for reduction of MC in [21] but this decoupling structure uses extra space between the antennas. Double layer MTM mushroom wall in [22] and polarization-rotator wall in [23] are used for MC reduction in planar antennas and DRAs respectively though these methods increase the height and therefore vertical profile of the antenna array. Capacitively loaded loop based MTM superstrate and metasurface (MS)-based decoupling techniques are used for isolation enhancement in [24] and [25]. The decoupling in [26] is realized by adding a pure DB above the coupled array, and a ceramic superstrate in [27]. All these four designs have decoupling structures between or above the antenna elements, which significantly increase the antenna footprint. It is noted that the array antenna-decoupling surfaces (ADSs) or superstrates enable the partially reflected signal to interact out of phase with the coupled signal and hence nullify the effect of the latter thus ensuring better isolation. Intuitively, the height of the ADS above the antenna determines the phase of the partially reflected wave and the size of the metal reflection patches on the ADS controls the intensity of the partial reflected wave [28]. Therefore, ADSs or superstrates [29] are placed at some height above the antenna array that increase the overall height of the antenna.

In this paper, a novel single negative (SNG: μ and ϵ are of opposite signs) meta-grid line (MGL) structure is presented, which is used for the following two low MC MIMO antenna configurations:

1. Two-port coplanar waveguide (CPW)-fed monopole antenna array (TPCFMAA)
2. Two-port DRA array (TPDRAA)

The novel aspect presented in this article is the use of meta-grid lines (MGLs) integrated with the ground plane for suppression of the surface wave linkage between the antenna elements and hence achieve a satisfactory isolation level. Unlike EBGs, isolators or NLs for MC reduction, this approach obviates the need for any extra space between antennas to accommodate the decoupling unit. Also, integration of MGLs in the ground plane does not require any additional layers unlike ADSs or superstrates that increase the height of the antenna. Therefore, integration of MGLs in the ground plane helps to realize compact design and TPCFMAA has a minimal ($0.015\lambda_h$) edge-to-edge spacing between the antenna elements.

It is noted that for TPCFMAA, the unit cell periodicity (p) of MGL structure is 6.35 mm, guided wavelength (λ_g) is 57.7 mm whereas, for TPDRAA, p is 6 mm, λ_g is 34.85 mm at 5.8 GHz. Hence, p is much smaller than the guided wavelength λ_g of the propagating wave (i.e. $p \ll \lambda_g$) [30], [31], so that fields are averaged across the unit cells and see the structure as a homogenous medium at a macroscopic scale. Also, from the extracted permittivity and permeability curves of MGLs for TPCFMAA and TPDRAA, it is noted that the MGLs shows wideband SNG behaviour. Therefore, although the presented structure bears resemblance to a DGS (both being etched copper patterns on the ground plane), due to the characteristic properties discussed above, the former is significantly different from a DGS that uses slot (of length comparable to the guided wavelength [32], [33] or half of the guided wavelength [34]).

It may also be noted that most of the MC reduction techniques employing EBG and superstrates do not generally show portability or interoperability among different types of radiators (patch antenna↔DRA). This means that EBG and superstrates for MC reduction in patch antennas are generally very difficult to be employable in DRAs without major modifications in their structures and vice-versa. However, this is not the case with presented technique because in TPDRAA, the dielectric blocks are excited by means of microstrip patch feed which are printed over an MGL (with wideband SNG characteristics) backed substrate. Therefore, MGLs effectively deal with the MC in both printed and dielectric resonator antennas. One may also note that an important feature of this decoupling structure is that by varying its geometric parameter, it is possible to make the TPCFMAA resonate over a wide range of frequencies while ensuring minimal offset between the return loss and mutual coupling i.e. the antenna resonating frequency can be positioned at any value lying from 2.6 to 4.4 GHz keeping the MC performance undisturbed. In the TPDRAA design as well, the

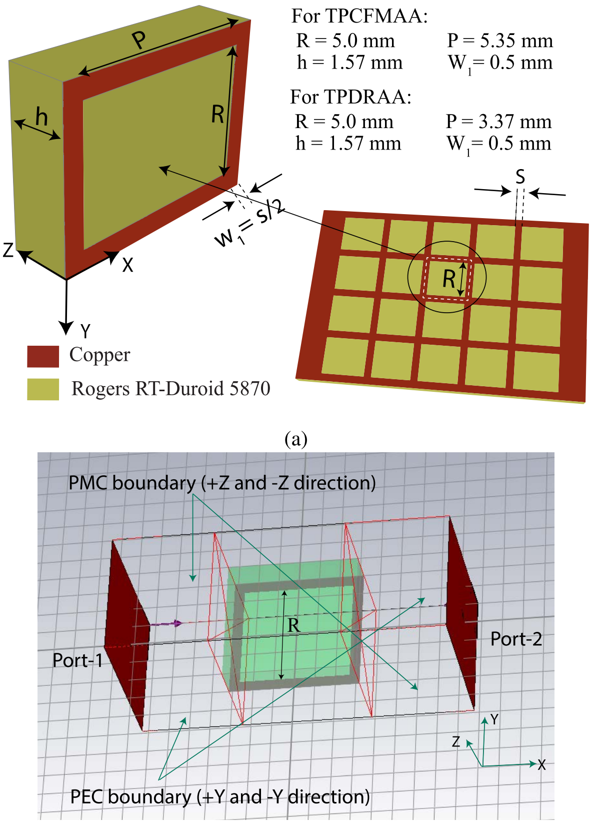

(a)

(b)

FIGURE 1. Meta-grid lines in the ground plane (a) unit cell (b) simulation set-up for effective material parameter extraction.

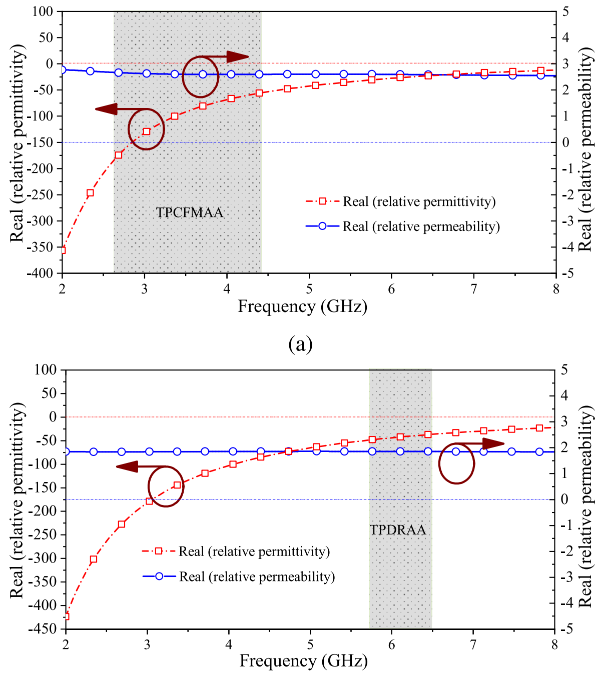

(a)

(b)

FIGURE 2. Extracted effective permittivity and permeability of the unit cell for (a) TPCFMAA and (b) TPDRAA.

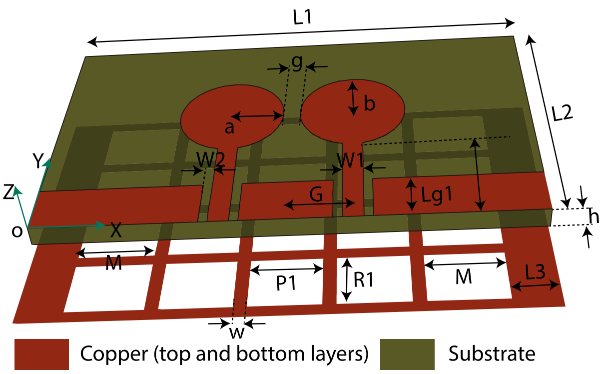

FIGURE 3. Geometry of 2-port CPW-fed monopole antenna array.

resonating frequency can be made to lie at any value between 5.78 and 6.55 GHz by changing the dimensions of annular ring slots in the patch which excites the DRA. Even in the TPDRAA, the MC performance is preserved with varying antenna resonating frequency.

Section II presents the unit cell analysis of the proposed MGL structure. Section III contains the TPCFMAA, Section IV discusses the TPDRAA. Conclusions are drawn in Section V.

II. UNIT CELL ANALYSIS

An isolated unit cell (single unit cell) of MGLs integrated with the ground plane is shown in Fig. 1(a). The MGLs are printed on the back of Rogers RT-Duroid 5870 with $\epsilon_r = 2.33$ and $\tan(\delta) = 0.0012$. The simulation set-up illustrating wave-guide ports and boundary conditions for extracting the real parts of the complex permeability and permittivity of such a unit cell is shown in Fig. 1(b). Permeability and permittivity curves are plotted in Fig. 2(a) and Fig. 2(b) using parameter retrieval option in CST Microwave Studio Suite 2018.

From Fig. 2(a) and Fig. 2(b), it can be seen that the unit cell shows the behavior of SNG MTM (ϵ-negative). Refractive index ($n = \sqrt{\mu\epsilon}$) becomes imaginary if μ and ϵ are of opposite sign. Electromagnetic waves can not propagate in such mediums, and therefore can be used for the isolation enhancement in the multi-port MIMO antennas by suppressing the propagation of the surface waves from one antenna to another. Gray shaded regions in Fig. 2(a) and Fig. 2(b) indicate the operating frequency ranges of TPCFMAA and TPDRAA respectively.

III. 2-PORT CPW-FED PLANAR MONOPOLE ANTENNA ARRAY USING SNG META-GRID LINES

In this section, a TPCFMAA employing the SNG MGLs integrated with the ground plane for MC reduction shown in Fig. 3 is discussed. The values of all the geometrical dimensions (in mm) corresponding to Fig. 3 are given below: L1 = 38.75, L2 = 25, P1 = 5.35, R1 = 5, G = 5, a = 4.8, b = 4.32, w = 1, Lg1 = 4.5, L3 = 3.5, W1 = 1.6, W2 = 0.7, r = a/b.

The top layer consists of two CPW-fed elliptical printed monopole patches which are used as radiators whereas the

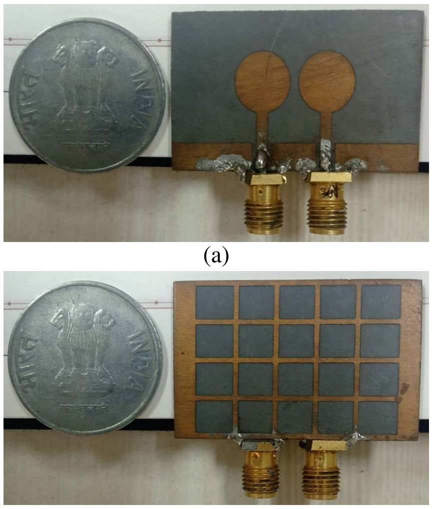

(a)

(b)

FIGURE 4. Fabricated prototype of 2-port CPW-fed monopole antenna array (a) top view and (b) bottom view.

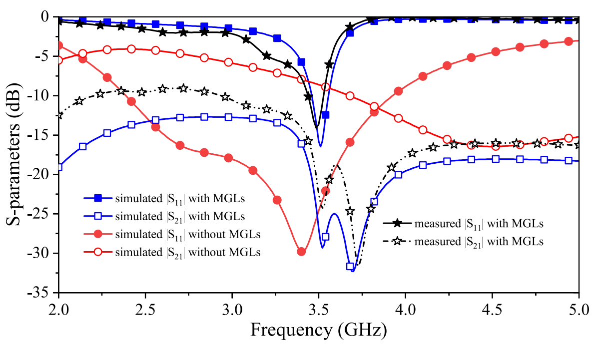

FIGURE 5. S-parameters with and without MGLs integration in ground plane.

bottom layer consists of a MGL structure (5 × 4 unit cells). The photographs of the top view and the bottom view of the fabricated prototype of TPCFMAA are shown in Fig. 4(a) and Fig. 4(b), respectively. All simulation results are generated using High-frequency structure simulator (HFSS) 14.0. To understand the contribution of the proposed MGL structure in MC reduction, the S-parameters without and with this structure are plotted in Fig. 5. It is apparent from these plots that integrating the MGLs in the ground plane at 3.5 GHz reduces the MC by 20 dB. MGLs reduces MC at the expense of reduction in antenna bandwidth. Two important design parameters (M and G as in Fig. 3) are found to be vital in positioning the antenna resonating frequency. In case of G as shown in Fig. 6, increasing or decreasing the values of G shift the frequency upward or downward respectively. However, in case of M as shown in Fig. 7, it is reversed, i.e. increasing or decreasing the values of M shift the frequency downward or upward respectively. In both the cases, the MC performance remains intact. Retaining the MC performance with varied resonating frequencies is one of the novel aspects of proposed two-port antenna. For M = 6.85 mm and G = 5 mm, the antenna can be designed for 3.5 GHz WiMAX application.

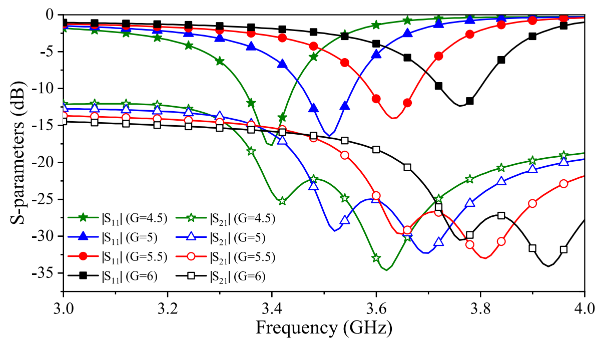

FIGURE 6. S-parameters for different values of G.

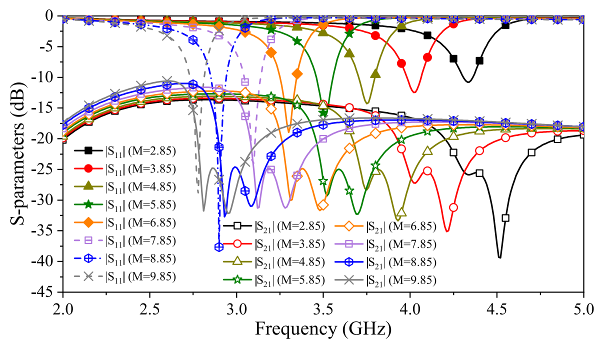

FIGURE 7. S-parameters for different values of M.

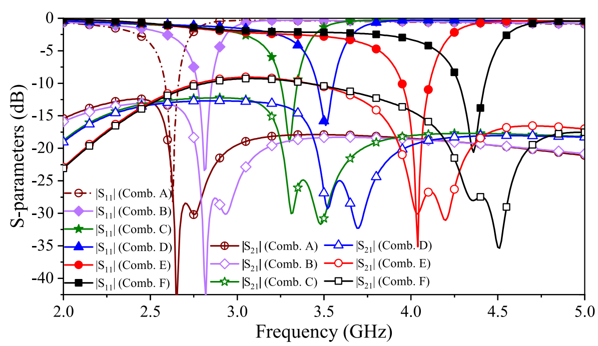

FIGURE 8. S-parameters for the various combinations of the M, G and r.

At 3.5 GHz design frequency, the electrical size of the antenna is noted to be 0.45 $\lambda_0 \times 0.30\lambda_0$.

Fig. 8 shows the S-parameter variations corresponding to the various combinations of the M, G and r named as Combination A (M = 12.85, G = 7, r = 0.9), Combination B (M = 11.85, G = 7, r = 0.9), Combination C (M = 9.85, G = 5, r = 0.9), Combination D (M = 5.85, G = 5, r = 0.9), Combination E (M = 3.85, G = 5, r = 0.3) and Combination F (M = 2.85, G = 5, r = 0.3). It is seen that by selecting the proper combination of these parameters, optimum mutual coupling performance can be obtained and the antenna can be designed to resonate at any frequency from 2.6 GHz to 4.4 GHz. For example, using Combination B (M = 11.85, G = 7, r = 0.9) isolation close to −45 dB can be achieved. For Combination A, the MC is below −17.27 dB while for rest of the combinations, the MC is noted to be below −20 dB.

Table 1 shows that the proposed TPCFMAA has the minimum inter-element spacing (λ_h) except that in [25]

TABLE 1. Comparison of the proposed TPCFMAA with other EBG, MTM, MS and DB based two-port antenna designs.

Ref.	Bandwidth (GHz)	Size (λ_h^3)	Multi-Layer	Excess height	Edge to edge spacing	Mutual Coupling
[7]	5.75 center frequency, bandwidth not mentioned	1.50×1.50×0.049	Yes	1.27 mm	$0.5\lambda_h$	$\leq$ -20 dB
[8]	4.85-5.08	0.87×0.43×0.024	No	0.00 mm	$0.13\lambda_h$	$\leq$ -23 dB
[9]	8.7-11.7, 11.9-14.6, 15.6-17.1,22-26,29-34.2	1.07×2.03×0.046	No	0.00 mm	$0.58\lambda_h$	$\leq$ -28 dB
[24]	3.3 to 3.34	1.6×0.9×0.16	Yes	14.3 mm	$0.12\lambda_h$	$\leq$ -40 dB
[25]	2.5-2.7, 3.4-3.6	0.83×1.25×0.14	Yes	11 mm	$0.008\lambda_h$	$\leq$ -25 dB
[26]	4.6-5.29	1.53×0.92×0.38	Yes	16.5 mm	$0.092\lambda_h$	$\leq$ -20 dB
[27]	3.3-3.7	1.1×1.1×0.385	Yes	35 mm	$0.264\lambda_h$	$\leq$ -25 dB
TPCFMAA	3.46-3.56	0.28×0.45×0.018	No	No extra height	$0.015\lambda_h$	$\leq$ -20 dB

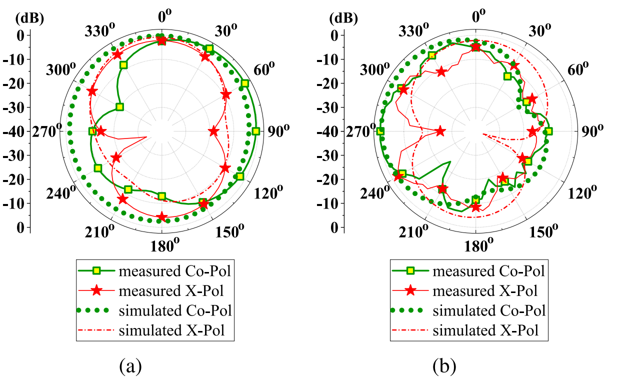

FIGURE 9. Radiation patterns for (a) $\phi = 0^0$ plane and (b) $\phi = 90^0$ plane.

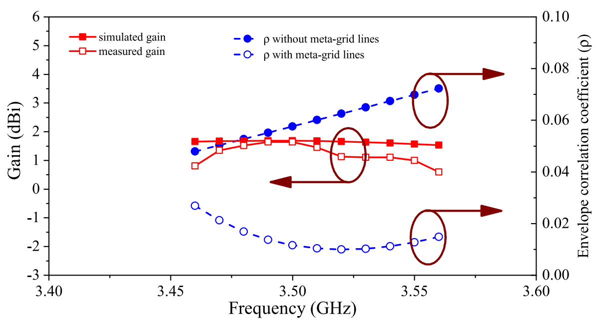

FIGURE 10. Measured and simulated gain, ECC of the TPCFMAA.

but [25] occupies 64 times more volume (in λ_h^3) than TPCFMAA. The TPCFMAA has broader percentage bandwidth than [24], comparable percentage bandwidth with [7] but lesser percentage bandwidth than [8], [9], [25], [26] and [27]. However, excellent bandwidth improvements will be shown for TPDRAA employing meta-grid lines in the ground plane as discussed in section IV. The TPCFMAA is a very low profile antenna which occupies 48.6, 3.95, 44, 101.6, 64, 236 and 205 times lower volume than that of [7]–[9], [24]–[27], respectively. In fact, elements of this highly compact MIMO antenna satisfy criterion ($ka < 1$) for electrically small antennas [35]. Furthermore, the TPCFMAA design is simple, compact and especially, does not have a multi-layer arrangement contrary to the antennas of [7], [24]–[27] that add excess heights to these antenna profiles.

Normalized radiation patterns at 3.5 GHz (Combination D) for $\phi = 0^0$ plane and $\phi = 90^0$ plane are plotted in Fig. 9. The peak gain is noted to be lying from 1.53 dBi to 1.68 dBi within the antenna bandwidth from 3.46 GHz to 3.56 GHz (Fig. 10). It can be observed that the measured gain slightly deviates from the simulated gain which may be due to fabrication tolerances.

The ECC is a measure of isolation and correlation between communication channels and is an important performance metric to be considered in MIMO communication. The ECC between the antenna ports is calculated using equation (1) from [36] and plotted in Fig. 10.

$$\rho_{ij} = \frac{\left| \iint_{4\pi} \left[\vec{F}_i(\theta,\phi) * \vec{F}_j(\theta,\phi) \right] d\Omega \right|^2}{\left(\iint_{4\pi} \left| \vec{F}_i(\theta,\phi) \right|^2 d\Omega \right) \left(\iint_{4\pi} \left| \vec{F}_j(\theta,\phi) \right|^2 d\Omega \right)} \quad (1)$$

Here, $\vec{F}_i(\theta,\phi)$ is simulated 3-D radiation field corresponding to the i^{th} antenna element and Ω is the solid angle.

It is obvious from Fig. 10 that the ECC is significantly reduced from 0.072 to 0.026 over the entire operation band when MGLs are integrated in the ground plane. The ECC for the TPCFMAA is found to be below 0.026 within the operational bandwidth. The antenna correlation coefficient (ACC) is approximately equal to the square root of the ECC [37]. Hence, the ACC matrix of this two-element MIMO antenna is $\begin{pmatrix} 1 & 0.161 \\ 0.161 & 1 \end{pmatrix}$. The channel capacity loss (CCL) [38] for point-to-point N × N MIMO system is

$$CCL = -log_2(det(\mathbf{R_{Rx}})) - log_2(det(\mathbf{R_{Tx}})), \quad (2)$$

where $\mathbf{R_{Rx}}$ and $\mathbf{R_{Tx}}$ are the ACC matrix of the MIMO antenna deployed at the transmitter and the receiver respectively. For a 2 × 2 MIMO system deploying two-element MIMO antenna of Fig. 3 at the transmitter as well as at the receiver, the CCL is calculated to be just 0.0758 b/s/Hz. Such a low CCL is a desirable characteristic of MIMO antenna. Since the ACC matrix for this MIMO antenna is full rank (rank = 2), 2 × 2 MIMO system deploying the TPCFMAA will achieve maximum diversity gain of 4.

Considering the practical deployment of this antenna and to understand the effect of the large ground plane on antenna performance, simulation with an extended ground plane (50 mm in the +Y axis, +X axis and -X axis direction as per Fig. 3) in the plane containing the bottom layer of the antenna is carried out. It is noted that the cross-polarization discrimination (XPD) performance and antenna gain both improve with the usage of extended ground plane. Another simulation is carried out with a large ground plane (50 mm

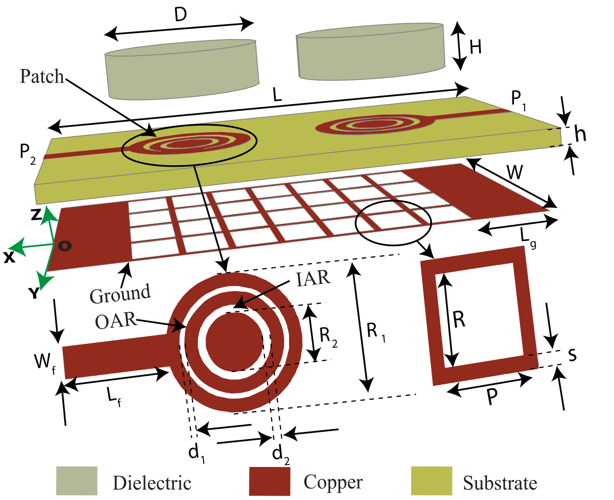

FIGURE 11. Antenna geometry: 2-port DRA array.

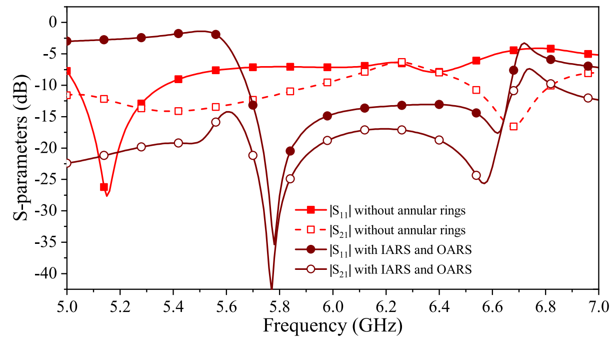

FIGURE 12. S-parameters without annular rings and with both annular rings.

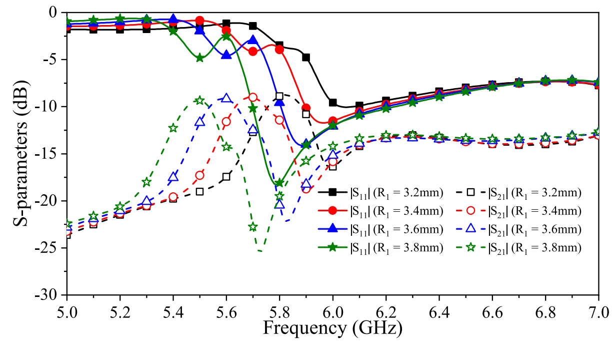

FIGURE 13. S-parameters for different values of radius for the OARS.

in the +Y axis, +X axis and -X axis direction as per Fig. 3), which is placed 10 mm below the plane containing the bottom layer of the TPCFMAA. It is seen that the gain improves from 1.65 dBi to 2.91 dBi. However, the XPD does not improve. In both the cases, impedance matching and isolation performances remain almost unaffected.

The TPCFMAA can be mounted over a vehicle roof where it can utilize the large metallic roof of the vehicle as extended large ground plane or as a reflector below the antenna. Therefore, this antenna can be used for the 3.5 GHz Internet of Vehicles (IoV) multi-user MIMO service.

IV. 2-PORT DRA ARRAY USING SNG META-GRID LINES

This section contains the TPDRAA as shown in Fig. 11. It uses two CDRA blocks of $\epsilon_r = 25$ as radiating elements. These dielectric blocks are excited by means of two concentric annular rings in the circular patches placed above the substrate (Rogers RT-Duroid 5870 with $\epsilon_r = 2.33$ and $\tan(\delta) = 0.0012$). These circular patches are connected to the microstrip line through which signal is fed to the antenna elements. The ground plane (in maroon) has an MGL structure (7×4 unit cells) integrated between two uniform rectangular sections of dimensions $L_g \times W$ at its two ends. The values of all the geometrical dimensions (in mm) corresponding to Fig. 11 are: D = 14.4, H = 3.8, L = 45, W = 25, $L_g = 7.2$, $W_f = 2.4$, $L_f = 7.7$, $R_2 = 4.4$, $R_1 = 10.4$, P = 3.37, R = 5, $d_1 = 0.4$, $d_2 = 0.6$, s = 1, h = 1.57.

Using equations (3) and (4) from [39], resonating frequency of the circular patch of radius a = 5.2 mm is calculated to be 9.8 GHz which is much higher than the frequency range of the proposed antenna. Therefore, it is concluded that the non-radiating patches with annular ring slots are used for exciting the $HEM_{12\delta}$ mode in the cylindrical dielectric blocks.

$$F = \frac{8.791 \times 10^9}{f_r \times \sqrt{\epsilon_r}} \tag{3}$$

$$a = \frac{F}{\sqrt{1 + \frac{2h}{\epsilon_r \pi F}(\log_e(\frac{\pi F}{2h} + 1.7726))}} \tag{4}$$

Here, h and a are in cm and f_r is the resonant frequency of the circular patch.

Without annular ring slots, the bandwidth of the antenna is noted to be very less (refer Fig. 12). This is mainly because of high dielectric constant of CDRA blocks i.e. 25. Therefore, attempts are made to increase the bandwidth of the antenna by employing the annular ring slots in the circular patch to excite the CDRA blocks.

It is clearly shown in [40] that increasing the radius of the feeding slot decreases the resonating frequency and vice-versa. The same is noted in the S-parameters of the antenna with only the outer annular ring slot (OARS) and only the inner annular ring slot (IARS) by varying the radius of the slots, which are plotted in Fig. 13 and Fig. 14 respectively. It has been observed that by varying the radius of OARS and IARS, the resonance can be adjusted in the lower frequency region and higher frequency region respectively. By choosing the radius of the OARS as 3.8 mm and IARS as 2.2 mm, the bandwidth of the antenna can be significantly increased when compared to the excitation of the DRA blocks without the annular slots in the circular patch. It can be inferred from Fig. 12 that the lower resonance occurring at 5.78 GHz is because of the OARS and the higher resonance at 6.5 GHz is because of the IARS. When both the IARS and the OARS are used together, these two resonances merge and lead to a wider bandwidth from 5.68 GHz to 6.7 GHz as shown in Fig. 12.

The dimensions of the circular dielectric block to excite the $HEM_{12\delta}$ at the 5.8 GHz, is calculated using equation (5) from [41] and turn out to be $H = 3.8$ mm

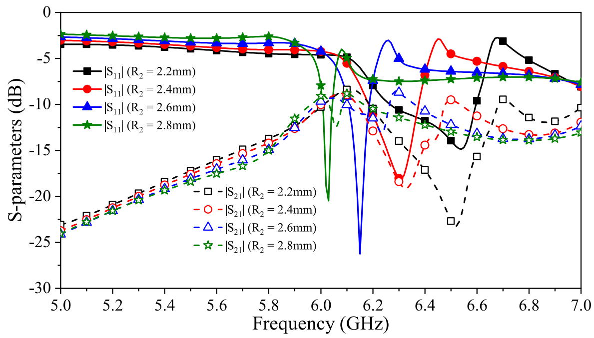

FIGURE 14. S-parameters for different values of radius for the IARS.

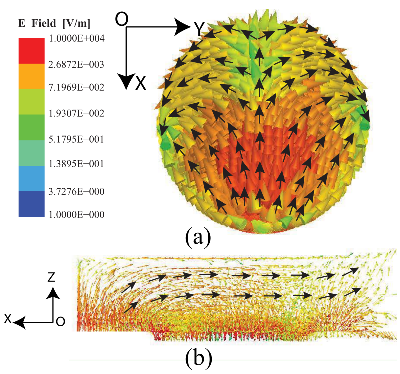

FIGURE 15. Electric field distribution at 5.78 GHz for (a) top and (b) side view.

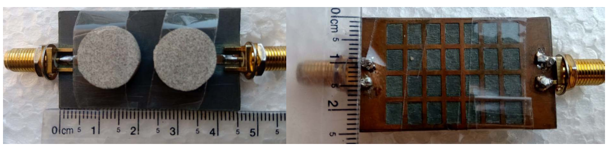

FIGURE 16. Fabricated antenna prototype (top and bottom views).

and $D = 14.4$ mm.

$$f(GHz) = \frac{30k_0 a}{2\pi a(cm)} \tag{5}$$

where,

$$k_0 a = \frac{3.72 + 0.4464x + 0.2232x^2 + 0.0521x^3 - 2.65\exp^{-N}}{\sqrt{\epsilon_r}}$$

$a = \frac{D}{2}, x = \frac{a}{2H}$ and $N = 1.25x(1 + 4.7x)$, f is the resonating frequency and ϵ_r is the relative permittivity of DRA.

From Fig. 13, it is observed that the mutual coupling curves have valleys just below the resonance for the OARS and same is observed for the IARS in Fig. 14. This is mainly because of the integration of the MGLs in the ground plane.

Electric field patterns at 5.78 GHz are shown in Fig. 15 and confirms the excitation of $HEM_{12\delta}$ mode [42].

The simulated and measured S-parameters versus frequency of the fabricated prototype (as depicted in Fig. 16) are plotted in Fig. 17. The measured impedance bandwidth of the antenna is observed to lie from 5.65 GHz to 6.55 GHz, whereas the simulated bandwidth is from 5.68 GHz to 6.7 GHz. The slight difference in the measured and simulated bandwidth of this antenna is because of various tolerances such as imperfections in the cutting of DRA blocks and PCB fabrication. The measured isolation between the antenna elements is found to be more than 16 dB for the entire bandwidth and the maximum isolation is noted to be 38.6 dB.

The measured and simulated co-polar and cross-polar radiation patterns for $\phi = 0^0$ and $\phi = 90^0$ planes at 5.8 GHz are plotted in Fig. 18. During pattern measurements, port P_1 is excited whereas port P_2 is terminated with a matched load. The measured cross-polarization discrimination (XPD) in the broadside direction is greater than 11.5 dB in both planes. The difference in the cross polarized results between simulation and experiment could be due to the detector sensitivity. The measured and the simulated gain with respect to frequency are plotted in Fig. 19. Peak measured gain is noted to be from 4.17 dBi to 5.2 dBi, while the simulated gain is observed to lie between 3.97 dBi and 5.4 dBi.

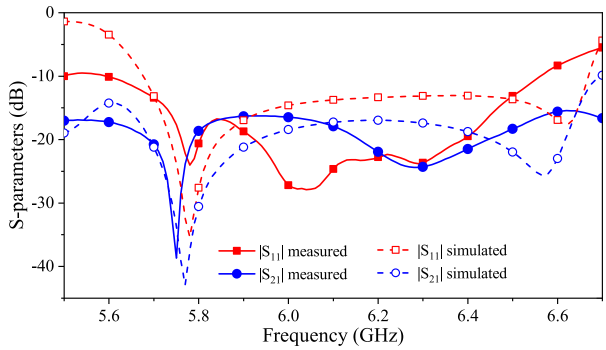

FIGURE 17. Measured and simulated S-parameters.

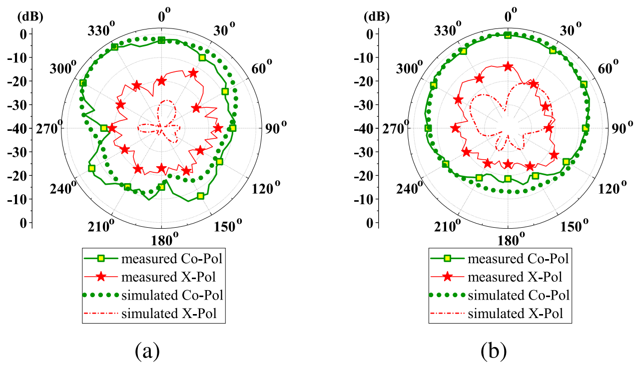

FIGURE 18. Radiation patterns for (a) $\phi = 0^0$ plane and (b) $\phi = 90^0$ plane.

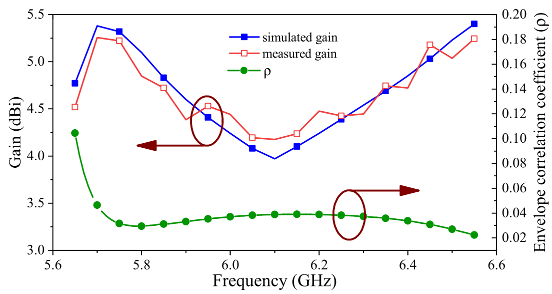

FIGURE 19. Measured, simulated gain and ECC of the MIMO antenna.

TABLE 2. Comparison of the proposed work with the state of the art.

References	Bandwidth (GHz)	Antenna size (λ_h^3)	No. of ports	Inter-element spacing (λ_h)	Mutual Coupling
[16]	5.15-6	1.03×0.68×0.148	3	$0.291\lambda_h$	$\leq$ -20 dB
[18]	9.04-9.92	1.7×1.7×0.424	3	Not applicable	$\leq$ -18 dB
[19]	27.25-28.35	1.8×1.8×0.25	2	$0.117\lambda_h$	$\leq$ -24 dB
[20]	25.2-27.1	1.8×0.92×0.13	2	$0.11\lambda_h$	$\leq$ -30 dB
This work	5.65- 6.55	0.84×0.46×0.091	2	$0.091\lambda_h$	$\leq$ -16 dB

The ECC as a function of the frequency is plotted in Fig. 19 and its value is noted to be < 0.046 in the entire operating frequency range of the antenna array. Hence, the ACC matrix of this two-element MIMO antenna is $\begin{pmatrix} 1 & 0.214 \\ 0.214 & 1 \end{pmatrix}$. For a 2×2 MIMO system deploying two-element MIMO antenna of Fig. 11, the CCL is calculated to be 0.1727 b/s/Hz, which is low and desirable. The ACC matrix of this MIMO antenna is full rank (rank = 2) and hence 2×2 MIMO system employing the TPDRAA will achieve maximum diversity gain of 4.

The comparison of the proposed work (TPDRAA) with other contemporary works is listed in Table 2. It has been observed that MIMO antennas in [16], [18]–[20] occupy 3, 34.8, 23 and 6.1 times more volumes than the TPDRAA, respectively. Moreover, the TPDRAA has the largest percentage bandwidth except [16] and the lowest inter-element spacing (in terms of λ_h).

V. CONCLUSION

In this paper, meta-grid lines are integrated in the ground plane for effectively reducing the MC in a TPCFMAA which is further extended for MC reduction in case of a TPDRAA as well. The proposed MC reduction approach does not add any extra foot print to the TPCFMAA and the TPDRAA profile. The TPCFMAA and the TPDRAA are fabricated and tested as proofs-of-concept. For the TPCFMAA, at 3.5 GHz center frequency (bandwidth from 3.46 GHz to 3.56 GHz), the MC is -28 dB and the ECC is below 0.026. Therefore, the TPCFMAA is a suitable candidate for 2-port MIMO WiMAX application. The MC in the TPDRAA, is noted to be less than -16 dB with the ECC less than 0.046, therefore satisfying the criteria of low correlation, making this compact TPDRAA a suitable candidate for MIMO application in the operating frequency range from 5.65 GHz to 6.55 GHz that covers 5.925 to 6.425 GHz frequency band for satellite communication, 5.7 to 5.85 GHz for WiMAX, 5.725 to 5.85 GHz for ISM band and 5.8 GHz for WLAN application.

ACKNOWLEDGMENT

Mohit Mishra, Sumantra Chaudhuri, and Rakhesh Singh Kshetrimayum are thankful to Dr. Nemai Chandra Karmakar from Monash University, Australia, for his valuable comments and Rakhesh Singh Kshetrimayum is also grateful to Dr. Nasimuddin from I2R, A-STAR, Singapore, for some of his insightful comments. The authors are also grateful to the anonymous reviewers for their insightful comments and thoughtful suggestions, which helped them improve the quality of the article significantly.

REFERENCES

[1] R. S. Kshetrimayum, *Fundamentals MIMO Wireless Communication*. Cambridge, U.K.: Cambridge Univ. Press, 2017.

[2] M. A. Jensen and J. W. Wallace, "A review of antennas and propagation for MIMO wireless communications," *IEEE Trans. Antennas Propag.*, vol. 52, no. 11, pp. 2810–2824, Nov. 2004.

[3] H.-S. Lui, H. T. Hui, and M. S. Leong, "A note on the mutual-coupling problems in transmitting and receiving antenna arrays," *IEEE Antennas Propag. Mag.*, vol. 51, no. 5, pp. 171–176, Oct. 2009.

[4] K. Payandehjoo, A. Tavallaee, and R. Abhari, "Analysis of shielded electromagnetic bandgap structures using multiconductor transmission-line theory," *IEEE Trans. Adv. Packag.*, vol. 33, no. 1, pp. 236–245, Feb. 2010.

[5] F. Yang and Y. Rahmat-Samii, "Microstrip antennas integrated with electromagnetic band-gap (EBG) structures: A low mutual coupling design for array applications," *IEEE Trans. Antennas Propag.*, vol. 51, no. 10, pp. 2936–2946, Oct. 2003.

[6] F. Caminita, S. Costanzo, G. Di Massa, G. Guarnieri, S. Maci, G. Mauriello, and I. Venneri, "Reduction of patch antenna coupling by using a compact EBG formed by shorted strips with interlocked branch-stubs," *IEEE Antennas Wireless Propag. Lett.*, vol. 8, pp. 811–814, 2009.

[7] H. S. Farahani, M. Veysi, M. Kamyab, and A. Tadjalli, "Mutual coupling reduction in patch antenna arrays using a UC-EBG superstrate," *IEEE Antennas Wireless Propag. Lett.*, vol. 9, pp. 57–59, 2010.

[8] Y. Liu, X. Yang, Y. Jia, and Y. J. Guo, "A low correlation and mutual coupling MIMO antenna," *IEEE Access*, vol. 7, pp. 127384–127392, 2019.

[9] M. Alibakhshikenari, M. Khalily, B. S. Virdee, C. H. See, R. Abd-Alhameed, and E. Limiti, "Mutual coupling suppression between two closely placed microstrip patches using EM-bandgap metamaterial fractal loading," *IEEE Access*, vol. 7, pp. 23606–23614, 2019.

[10] Y.-F. Cheng, X. Ding, W. Shao, and B.-Z. Wang, "Reduction of mutual coupling between patch antennas using a polarization-conversion isolator," *IEEE Antennas Wireless Propag. Lett.*, vol. 16, pp. 1257–1260, 2016.

[11] M. Niroo-Jazi, T. A. Denidni, M. R. Chaharmir, and A. R. Sebak, "A hybrid isolator to reduce electromagnetic interactions between Tx/Rx antennas," *IEEE Antennas Wireless Propag. Lett.*, vol. 13, pp. 75–78, 2014.

[12] A. Cihangir, F. Ferrero, G. Jacquemod, P. Brachat, and C. Luxey, "Neutralized coupling elements for MIMO operation in 4G mobile terminals," *IEEE Antennas Wireless Propag. Lett.*, vol. 13, pp. 141–144, 2014.

[13] Y. Wang and Z. Du, "A wideband printed dual-antenna system with a novel neutralization line for mobile terminals," *IEEE Antennas Wireless Propag. Lett.*, vol. 12, pp. 1428–1431, 2013.

[14] D. Guha, S. Biswas, T. Joseph, and M. T. Sebastian, "Defected ground structure to reduce mutual coupling between cylindrical dielectric resonator antennas," *Electron. Lett.*, vol. 44, pp. 836–837, Jul. 2008.

[15] A. Sharma and A. Biswas, "Wideband multiple-input–multiple-output dielectric resonator antenna," *IET Microw., Antennas Propag.*, vol. 11, no. 4, pp. 496–502, Mar. 2017.

[16] G. Das, A. Sharma, R. K. Gangwar, and M. S. Sharawi, "Triple-port, two-mode based two element cylindrical dielectric resonator antenna for MIMO applications," *Microw. Opt. Technol. Lett.*, vol. 60, no. 6, pp. 1566–1573, Jun. 2018.

[17] A. Sharma, A. Sarkar, A. Biswas, and M. J. Akhtar, "A-shaped wideband dielectric resonator antenna for wireless communication systems and its MIMO implementation," *Int. J. RF Microw. Comput.-Aided Eng.*, vol. 28, no. 8, Oct. 2018, Art. no. e21402.

[18] A. Abdalrazik, A. S. A. El-Hameed, and A. B. Abdel-Rahman, "A three-port MIMO dielectric resonator antenna using decoupled modes," *IEEE Antennas Wireless Propag. Lett.*, vol. 16, pp. 3104–3107, 2017.

[19] Y. Zhang, J.-Y. Deng, M.-J. Li, D. Sun, and L.-X. Guo, "A MIMO dielectric resonator antenna with improved isolation for 5G mm-wave applications," *IEEE Antennas Wireless Propag. Lett.*, vol. 18, no. 4, pp. 747–751, Apr. 2019.

[20] Y. M. Pan, X. Qin, Y. X. Sun, and S. Y. Zheng, ''A simple decoupling method for 5G millimeter-wave MIMO dielectric resonator antennas,'' *IEEE Trans. Antennas Propag.*, vol. 67, no. 4, pp. 2224–2234, Apr. 2019.
[21] X. M. Yang, X. G. Liu, X. Y. Zhou, and T. J. Cui, ''Reduction of mutual coupling between closely packed patch antennas using waveguided metamaterials,'' *IEEE Antennas Wireless Propag. Lett.*, vol. 11, pp. 389–391, 2012.
[22] G. Zhai, Z. N. Chen, and X. Qing, ''Enhanced isolation of a closely spaced four-element MIMO antenna system using metamaterial mushroom,'' *IEEE Trans. Antennas Propag.*, vol. 63, no. 8, pp. 3362–3370, Aug. 2015.
[23] M. Farahani, J. Pourahmadazar, M. Akbari, M. Nedil, A. R. Sebak, and T. A. Denidni, ''Mutual coupling reduction in millimeter-wave MIMO antenna array using a metamaterial polarization-rotator wall,'' *IEEE Antennas Wireless Propag. Lett.*, vol. 16, pp. 2324–2327, 2017.
[24] A. Jafargholi, A. Jafargholi, and H. Jun Choi, ''Mutual coupling reduction in an array of patch antennas using CLL metamaterial superstrate for MIMO applications,'' *IEEE Trans. Antennas Propag.*, vol. 67, no. 1, pp. 179–189, Jan. 2019.
[25] F. Liu, J. Guo, L. Zhao, G.-L. Huang, Y. Li, and Y. Yin, ''Dual-band metasurface-based decoupling method for two closely packed dual-band antennas,'' *IEEE Trans. Antennas Propag.*, vol. 68, no. 1, pp. 552–557, Jan. 2020.
[26] M. Li, M. Y. Jamal, L. Jiang, and K. L. Yeung, ''Isolation enhancement for MIMO patch antennas sharing a common thick substrate: Using a dielectric block to control space-wave coupling to cancel surface-wave coupling,'' *IEEE Trans. Antennas Propag.*, vol. 69, no. 4, pp. 1853–1863, Apr. 2021.
[27] F. Liu, J. Guo, L. Zhao, G.-L. Huang, Y. Li, and Y. Yin, ''Ceramic superstrate-based decoupling method for two closely packed antennas with cross-polarization suppression,'' *IEEE Trans. Antennas Propag.*, vol. 69, no. 3, pp. 1751–1756, Mar. 2021.
[28] K.-L. Wu, C. Wei, X. Mei, and Z.-Y. Zhang, ''Array-antenna decoupling surface,'' *IEEE Trans. Antennas Propag.*, vol. 65, no. 12, pp. 6728–6738, Dec. 2017.
[29] J. Tang, F. Faraz, X. Chen, Q. Zhang, Q. Li, Y. Li, and S. Zhang, ''A metasurface superstrate for mutual coupling reduction of large antenna arrays,'' *IEEE Access*, vol. 8, pp. 126859–126867, 2020.
[30] R. Marques, F. Martin, and M. Sorolla, *Metamaterials With Negative Parameters: Theory, Design, and Microwave Applications*, Hoboken, NJ, USA: Wiley, 2011.
[31] D. Guha and Y. M. Antar, *Microstrip and Printed Antennas: New Trends, Techniques and Applications*. Hoboken, NJ, USA: Wiley, 2011.
[32] J. Ouyang, F. Yang, and Z. M. Wang, ''Reducing mutual coupling of closely spaced microstrip MIMO antennas for WLAN application,'' *IEEE Antennas Wireless Propag. Lett.*, vol. 10, pp. 310–313, 2011.
[33] M. A. Abdalla and A. A. Ibrahim, ''Compact and closely spaced metamaterial MIMO antenna with high isolation for wireless applications,'' *IEEE Antennas Wireless Propag. Lett.*, vol. 12, pp. 1452–1455, 2013.
[34] H. Xing, X. Wang, Z. Gao, X. An, H.-X. Zheng, M. Wang, and E. Li, ''Efficient isolation of an MIMO antenna using defected ground structure,'' *Electronics*, vol. 9, no. 8, p. 1265, Aug. 2020.
[35] H. A. Wheeler, ''Fundamental limitations of small antennas,'' *Proc. IRE*, vol. 35, pp. 1479–1484, Dec. 1947.
[36] A. Boukarkar, X. Q. Lin, Y. Jiang, L. Y. Nie, P. Mei, and Y. Q. Yu, ''A miniaturized extremely close-spaced four-element dual-band MIMO antenna system with polarization and pattern diversity,'' *IEEE Antennas Wireless Propag. Lett.*, vol. 17, pp. 134–137, 2018.
[37] M. S. Sharawi, ''Current misuses and future prospects for printed multiple-input, multiple-output antenna systems,'' *IEEE Antennas Propag. Mag.*, vol. 59, no. 2, pp. 162–170, Apr. 2017.
[38] Z. N. Chen, D. Liu, H. Nakano, X. Qing, and T. Zwick, *Handbook Antenna Technology*. Singapore: Springer, 2016, pp. 2356–2357.
[39] C. A. Balanis, *Antenna Theory Design*. Hoboken, NJ, USA: Wiley, 2015.
[40] C. Y. Huang and J. S. Kuo, ''Frequency-adjustable circularly polarized dielectric resonator antenna,'' *Microw. Opt. Tech. Lett.*, vol. 34, no. 3, pp. 211–213, 2002.
[41] K. Leung and K. Luk, *Dielectric Resonator Antenna*. Baldock, U.K.: Research Studies Press, 2003.
[42] D. Guha, A. Banerjee, C. Kumar, and Y. M. M. Antar, ''Higher order mode excitation for high-gain broadside radiation from cylindrical dielectric resonator antennas,'' *IEEE Trans. Antennas Propag.*, vol. 60, no. 1, pp. 71–77, Jan. 2012.

MOHIT MISHRA (Graduate Student Member, IEEE) received the B.Tech. degree in electronics and communication engineering from the Central University of Chhattisgarh, Bilaspur, Chhattisgarh, India, in 2014. He is currently pursuing the dual M.S.(Eng.) and Ph.D. degree with IIT Guwahati. His research interests include printed MIMO antennas and dielectric resonator antennas for MIMO applications. He is also an Active Member of the IEEE APS Society. He was a recipient of the 2021 COMSNETS Fellowship. He has served as the Chair for the IEEE Student Branch, IIT Guwahati, from May 2018 to July 2019, and during his tenure, the IEEE Kolkata Section's ''Best Student Branch Activity Award'' was presented to the IEEE Student Branch, IIT Guwahati, during ''STUDENT MEET'' at the IEEE TENSYMP-2019, Kolkata, India. He has held various key positions at the Students Gymkhana Council, including the Chairperson of the Students Senate and the Vice-President of the Students Gymkhana Council of IIT Guwahati.

SUMANTRA CHAUDHURI received the bachelor's degree in electronics and communication engineering from VTU, Belgaum, the M.S. degree in theoretical electrohydrodynamics (by research) from IIT Madras, and the Ph.D. degree from the Department of Electronics and Electrical Engineering, IIT Guwahati, in September 2020. He worked as an Application Engineer with COMSOL Multiphysics, in 2014. He is currently working as an Assistant Professor with the School of Engineering, Presidency University, Bengaluru. He has several publications in leading international journals and conferences to his credit. His domain of research is microwave antennas. He was a recipient of multiple international awards from reputed groups (Elsevier and Wiley) for his contributions as the author and a reviewer. He is also frequently approached by prestigious journals such as IEEE Transactions on Antennas and Propagation, *IET Microwaves, Antennas and Propagation*, and *AEU-International Journal of Electronics and Communication*, to serve as a Reviewer.

RAKHESH SINGH KSHETRIMAYUM (Senior Member, IEEE) received the B.Tech. degree in electrical engineering (EE) from IIT Bombay, India, in 2000, and the Ph.D. degree from the School of Electrical and Electronics Engineering (EEE), Nanyang Technological University, Singapore, in 2005.

Since 2005, he has been a Faculty Member with the Department of EEE, IIT Guwahati, where he was the Head of the Centre for Career Development, from 2018 to 2020, and is currently working as a Professor. He did postdoctoral research at the Department of EE, Pennsylvania State University, USA, in 2005; and the Department of Electrical Communication Engineering, Indian Institute of Science, Bengaluru, from 2004 to 2005. From 2000 to 2001, he worked as a Software Engineer with Mphasis, Pune. He has authored or coauthored four books and more than 140 papers in international journals and conference proceedings. His current research interests include antennas, RF circuit designs, and performance analysis for beyond 5G technologies.

Dr. Kshetrimayum is a fellow of IET, U.K. He has received multiple best paper awards, including the IEEE ANTS 2017 Best Paper Award (Third Prize). He is also an Editor of the IEEE Communications Letters and an Associate Editor of the IEEE Open Journal of Antennas and Propagation. He has also served on the Editorial Board of the IEEE Transactions on Microwave Theory and Techniques and the Program Committee of several international conferences, including IEEE GLOBECOM, IEEE ICC, and APMC. He had delivered several invited talks/tutorials on the topic ''MIMO antennas and its effects in MIMO wireless communications,'' at the IEEE Texas Symposium 2021, IEEE ANTEM 2021, and IEEE APACE 2021. He was the Session Chair/Co-Chair of ISAP 2021, APMC 2021, IEEE AP-S/URSI 2021, and IEEE DSP 2015; the TPC Chair (communication tracks) of NCC 2016; and the TPC Co-Chair of IEEE AEMC 2015. He has also served as an Advisor for the IEEE Guwahati Sub-Section in 2021.

AROKIASWAMI ALPHONES (Senior Member, IEEE) received the B.Tech. degree from the Madras Institute of Technology, Chennai, India, in 1982, the M.Tech. degree from IIT Kharagpur, Kharagpur, India, in 1984, and the Ph.D. degree in optically controlled millimeter-wave circuits from the Kyoto Institute of Technology, Kyoto, Japan, in 1992. From 1997 to 2001, he was with the Centre for Wireless Communications, National University of Singapore, Singapore, where he was involved in research on optically controlled passive/active devices. Since 2001, he has been with the School of Electrical and Electronic Engineering, Nanyang Technological University, Singapore. He has 35 years of research experience in the domain of microwaves and photonics. He has authored and presented over 300 technical papers in peer-reviewed international journals/conferences. His current research interests include electromagnetic analysis on planar RF circuits and integrated optics, microwave photonics, metamaterial-based leaky wave antennas, wireless power transfer technologies, and transceiver for 6G communication systems. He was involved in many IEEE flagship conferences held in Singapore. He was the General Chair of APMC 2009, MWP 2011, TENCON 2016, and APMC 2019. He was the Chairperson of the IEEE Singapore Section from 2015 to 2018 and a member of the IEEE Conference Quality Committee. He has been an invited plenary/extended/keynote speaker of several IEEE and other conferences and workshops held in various countries.

KARU P. ESSELLE (Fellow, IEEE) received the B.Sc. degree (Hons.) in electronic and telecommunication engineering from the University of Moratuwa, Sri Lanka, and the M.A.Sc. and Ph.D. degrees in near-perfect GPA in electrical engineering from the University of Ottawa, Canada.

He is currently a Distinguished Professor in electromagnetic and antenna engineering with the University of Technology Sydney and a Visiting Professor with Macquarie University, Sydney. According to the Special Report on research published by an Australian national newspaper, he is the 2019 National Research Field Leader in Australia in both microelectronics and electromagnetism fields. Previously, he was the Director of the WiMed Research Centre and the Associate Dean—Higher Degree Research (HDR) of the Division of Information and Communication Sciences, and the Centre for Collaboration in Electromagnetic and Antenna Engineering, Macquarie University. He has also served as a member for the Dean's Advisory Council, and the Division Executive and the Head for the Department several times. He is also the Director of Innovations for Humanity Pty Ltd. He has authored over 600 research publications, and his papers have been cited almost 12,000 times. In 2021, his publications received almost 1,300 citations. His H-index is 53 and i-10 is 203. He is in the world's top 100,000 most-cited scientists list by Mendeley Data. He has provided expert assistance to more than 12 companies, including Intel, Hewlett Packard Laboratory (USA), Cisco Systems (USA), Audacy (USA), Cochlear, Optus, ResMed, and Katherine-Werke (Germany). His team designed the high-gain antenna system for the world's first entirely Ka-band CubeSat made by Audacy, USA, and launched to space by SpaceX in December 2018. This is believed to be the first Australian-designed high-gain antenna system launched to space since CSIRO-designed antennas in Australia's own FedSat launched in 2002. Since 2002, his research team has been involved with research grants, contracts, and Ph.D. scholarships worth over 21 million dollars, including 16 Australian Research Council grants, without counting the 245 million-dollar SmartSat Corporative Research Centre, which started in 2019. His research has been supported by many national and international organizations, including the Australian Research Council, Intel, the U.S. Air Force, Cisco Systems, Hewlett-Packard, the Australian Department of Defence, the Australian Department of Industry, and German and Indian governments. His research activities are posted on the web at http://web.science.mq.edu.au/~esselle/ and https://www.uts.edu.au/staff/karu.esselle.

Dr. Karu is a fellow of the Royal Society of New South Wales and Engineers Australia. His awards include the 2021 Excellence Award—the most prestigious in 2021 Australian Defence Industry Awards, the 2021 Academic of the Year Award in the same, the 2021 IEEE Region 10 (Asia-Pacific) Outstanding Volunteer Award, the Finalist for 2021 Australian National Eureka Prize for Outstanding Mentor of Young Researchers, the Runner-Up to the same prize in 2020, the 2020 IEEE NSW Outstanding Volunteer Award, the 2019 Motohisa Kanda Award (from IEEE USA) for the Most Cited Paper in IEEE TRANSACTIONS ON ELECTROMAGNETIC COMPATIBILITY in the past five years, the 2019 Macquarie University Research Excellence Award for Innovative Technologies, the 2019 ARC Discovery International Award, the 2017 Excellence in Research Award from the Faculty of Science and Engineering, the 2017 Engineering Excellence Award for Best Innovation, the 2017 Highly Commended Research Excellence Award from Macquarie University, the 2017 Certificate of Recognition from IEEE Region 10, the 2016 and 2012 Engineering Excellence Awards for Best Published Paper from IESL NSW Chapter, the 2011 Outstanding Branch Counsellor Award from IEEE Headquarters (USA), the 2009 Vice Chancellor's Award for Excellence in Higher Degree Research Supervision, and the 2004 Innovation Award for Best Invention Disclosure. His mentees have been awarded many fellowships, awards, and prizes for their research achievements. Fifty-five international experts who examined the theses of his Ph.D. graduates ranked them in the Top 5% or 10%. Two of his students were awarded the Ph.D. degree with the highest honor at Macquarie University—the Vice Chancellor's Commendation, and one received the University Medal for Master of Research. From 2018 to 2020, he chaired the prestigious Distinguished Lecturer Program Committee of the IEEE Antennas and Propagation (AP) Society—the premier global learned society dedicated for antennas and propagation—which has close to 10,000 members worldwide. After two stages in the selection process, he was also selected by this society as one of two candidates in the ballot for the 2019 President of the Society. Only three people from Asia or Pacific apparently have received this honor in the 68-year history of this society. He is also one of the three distinguished lecturers (DL) selected by the society in 2016. He is the only Australian to chair the AP DL Program ever, the only Australian AP DL in almost two decades, and the second Australian AP DL ever (after UTS Distinguished Visiting Professor Trevor Bird). He has served the IEEE AP Society Administrative Committee in several elected or ex-officio positions from 2015 to 2020. He is also the Chair of the Board of Management of the Australian Antenna Measurement Facility, and was the Elected Chair of both the IEEE New South Wales (NSW), and IEEE NSW AP/MTT Chapter, in 2016 and 2017. He is in the College of Expert Reviewers of the European Science Foundation for the term 2019–2022, and has been invited to serve as an International Expert/Research Grant Assessor by several other research funding bodies, including the European Research Council, and funding agencies in Norway, Belgium, The Netherlands, Canada, Finland, Hong Kong, Georgia, South Africa, and Chile. He has been invited by the vice-chancellors of Australian and overseas universities to assess applications for promotion to professorial levels. He has also been invited to assess grant applications submitted to Australia's most prestigious schemes, such as Australian Federation Fellowships and Australian Laureate Fellowships. In addition to the large number of invited conference speeches he has given, he has been an Invited Plenary/Extended/Keynote Speaker of several IEEE and other conferences and workshops, including GSENN2022, Copenhagen, Denmark; EuCAP 2020, Copenhagen; EEEMEET 2022, Dubai; URSI 2019, Seville, Spain; and the 23rd ICECOM 2019, Dubrovnik, Croatia. He has served or is serving as an Associate Editor for IEEE TRANSACTIONS ON ANTENNAS AND PROPAGATION, *IEEE Antennas and Propagation Magazine*, and IEEE ACCESS. He is also the Track Chair of IEEE AP-S 2021 Singapore and AP-S 2020 Montreal; the Technical Program Committee Co-Chair of ISAP 2015, APMC 2011, and TENCON 2013; and the Publicity Chair of ICEAA/IEEE APWC 2016, IWAT 2014, and APMC 2000.